A mosaic of phytoplankton responses across Patagonia, the southeast Pacific and southwest Atlantic Oceans to ash deposition and trace metal release from the Calbuco volcanic eruption in 2015

Maximiliano J. Vergara-Jara[1,2], Mark J. Hopwood[3*], Thomas J. Browning[3], Insa Rapp[4], Rodrigo Torres[2,5], Brian Reid[5], Eric P. Achterberg[3], José Luis Iriarte[2,6].

[1]Programa de Doctorado en Ciencias de la Acuicultura, Universidad Austral de Chile, Puerto Montt, Chile.

[2]Instituto de Acuicultura & Centro de Investigación Dinámica de Ecosistemas Marinos de Altas Latitudes - IDEAL, Universidad Austral de Chile, Puerto Montt, Chile.

[3]GEOMAR, Helmholtz Centre for Ocean Research, 24148 Kiel, Germany.

[4]Department of Biology, Dalhousie University, Halifax, Nova Scotia, Canada

[5]Centro de Investigación en Ecosistemas de la Patagonia (CIEP), Coyhaique, Chile.

[6]COPAS-Sur Austral, Centro de Investigación Oceanográfica en el Pacífico Sur-Oriental (COPAS), Universidad de Concepción, Concepción, Chile.

Key words: volcanic ash, iron, Fe(II), phytoplankton, carbonate chemistry, Reloncaví Fjord

Corresponding author*: mhopwood@geomar.de

Abstract

Following the eruption of the Calbuco volcano in April 2015, an extensive ash plume spread across northern Patagonia and into the southeast Pacific and southwest Atlantic Oceans. Here we report on field surveys conducted in the coastal region receiving the highest ash load following the eruption (Reloncaví Fjord). The fortuitous location of a long-term monitoring station in Reloncaví Fjord provided data to evaluate inshore phytoplankton bloom dynamics and carbonate chemistry during April-May 2015. Satellite derived chlorophyll-a measurements over the ocean regions affected by the ash plume in May 2015 were obtained to determine the spatial-temporal gradients in offshore phytoplankton response to ash. Additionally, leaching experiments were performed to quantify the release from ash into solution of total alkalinity, trace elements (dissolved Fe, Mn, Pb, Co, Cu, Ni and Cd) and major ions (Fl^-, Cl^-, SO_4^{2-}, NO_3^-, Li^+, Na^+, NH_4^+, K^+, Mg^{2+}, Ca^{2+}). Within Reloncaví Fjord, integrated peak diatom abundances during the May 2015 austral bloom were approximately 2-4 times higher than usual (up to 1.4×10^{11} cells m^{-2}, integrated to 15 m depth), with the bloom intensity perhaps moderated due to high ash loadings in the two weeks following the eruption. Any mechanistic link between ash deposition and the Reloncaví diatom bloom can however only be speculated on due to the lack of data immediately preceding and following the eruption. In the offshore southeast Pacific, a short duration phytoplankton bloom corresponded closely in space and time to the maximum observed ash plume, potentially in response to Fe-fertilization of a region where phytoplankton growth is typically Fe-limited at this time of year. Conversely, no clear fertilization on the same time-scale was found in the area subject to an ash plume over the southwest Atlantic where the availability of fixed nitrogen is thought to limit phytoplankton growth. This was consistent with no significant release of fixed nitrogen (NO_x or NH_4) from the ash.

In addition to release of nanomolar concentrations of dissolved Fe from ash suspended in seawater, it was observed that low loadings (< 5 mg L^{-1}) of ash were an unusually prolific source of Fe(II) into chilled seawater (up to 1.0 µmol Fe g^{-1}), producing a pulse of Fe(II) typically released mainly during the first minute after addition to seawater. This release would not be detected, either as Fe(II) or dissolved Fe, following standard leaching protocols at room temperature. A pulse of Fe(II) release upon addition of Calbuco ash to seawater made it an unusually efficient dissolved Fe source with the ~18-38% fraction of dissolved Fe released as Fe(II) from Calbuco ash roughly comparable to literature values for Fe released into seawater from aerosols collected over the Pacific Ocean which have been substantially moderated by photochemical processing.

1. Introduction

Volcanic ash has long been considered a large, intermittent source of trace metals to the ocean (Frogner et al., 2001; Sarmiento, 1993; Watson, 1997) and its deposition is now deemed a sporadic generally low-macronutrient, high-micronutrient supply mechanism (Ayris and Delmelle, 2012; Jones and Gislason, 2008; Lin et al., 2011). As volcanic ash can be a regionally significant source of allochthonous inorganic material to affected water bodies, volcanic eruptions have the potential to dramatically change light availability, the carbonate system, properties of sinking particles and ecosystem dynamics (Hoffmann et al., 2012; Newcomb and Flagg, 1983; Stewart et al., 2006). Surveys directly underneath the ash plume from the 2010 eruption of Eyjafjallajökull (Iceland) over the North Atlantic found, among other biogeochemical perturbations, high dissolved Fe (dFe) concentrations of up to 10 nM in affected surface seawater (Achterberg et al., 2013) which could potentially result in enhanced primary production. The greatest potential positive effect of ash deposition on marine productivity would generally be expected in high-nitrate, low-chlorophyll (HNLC) areas of the ocean (Hamme et al., 2010; Mélançon et al., 2014), where low Fe concentrations are a major factor limiting primary production (Martin et al., 1990; Moore et al., 2013). Special interest is therefore placed on the ability of volcanic ash to release dFe, and other bio-essential trace metals such as Mn (Achterberg et al., 2013; Browning et al., 2014; Hoffmann et al., 2012), into seawater. In contrast, apart from inducing light limitation, there are several adverse effects of ash deposition on aquatic organisms. These include metal toxicity (Ermolin et al., 2018), particularly under high dust loading (Hoffmann et al., 2012), and the ingestion of ash particles by filter feeders, phagotrophic organisms or fish (Newcomb and Flagg, 1983; Wolinski et al., 2013). Transient shifts to low pH have also been reported in some, but not all, ash leaching experiments and in some fresh waterbodies following

intense ash falls, suggesting that significant ash deposition on weakly buffered aquatic environments can also impact and perturb their carbonate system (Duggen et al., 2010; Jones and Gislason, 2008; Newcomb and Flagg, 1983). The greatest negative impact of ash on primary producers would therefore be expected closest to the source where the ash loading is highest and in areas where macronutrients or light, rather than trace elements, limit primary production.

In contrast to the North Atlantic 2013 Eyjafjallajökull plume over the North Atlantic, the 2015 ash plume over the region from the Calbuco eruption (northern Patagonia, Chile) was predominantly deposited largely over an inshore and coastal region (Romero et al., 2016) (Fig. 1). This led to visible high ash loadings in affected surface waters in the weeks after the eruption (Fig. 2), providing a case study for a concentrated ash deposition event in a coastal system; Reloncaví Fjord, which is the northernmost fjord of Patagonia. It receives the direct discharge from three major rivers, creating a highly stratified and productive fjord system in terms of both phytoplankton biomass and aquaculture production of mussels (González et al., 2010; Molinet et al., 2017; Yevenes et al., 2019). Here we combine in situ observations from moored arrays which were fortuitously deployed in Reloncaví Fjord (Vergara-Jara et al., 2019), with satellite-derived chlorophyll data for offshore regions subject to ash deposition, and leaching experiments to investigate the inorganic consequences of ash addition to solution. We thereby evaluate the potential positive and negative effects of ash from the 2015 Calbuco eruption on marine primary production in three geographical regions; Reloncaví Fjord and the areas of the SE Pacific and SW Atlantic Oceans beneath the most intense ash plume.

2. **Materials and methods**

2.1. *Study area*

The Calbuco volcano (Fig. 1) is located in a region with large freshwater reservoirs and a major river (the Petrohué) that flows into Reloncaví Fjord. The predominant bedrock type is andesite (López-Escobar et al., 1995). Reloncaví Fjord is 55 km long and receives freshwater from 3 main rivers, the Puelo, Petrohué, and Cochamó, with mean stream flows of 650 $m^3 s^{-1}$, 350 $m^3 s^{-1}$ and 100 $m^3 s^{-1}$, respectively (León-Muñoz et al., 2013). River discharge strongly influences seasonal patterns of primary production across the region, supplying silicic acid and strongly stratifying the water column (Castillo et al., 2016; González et al., 2010; Torres et al., 2014). Seasonal changes in light availability rather than macronutrient supply are thought to control marine primary production across the Reloncaví region with high marine primary production (>1 g C m^{-2} day^{-1}) throughout austral spring, summer and early autumn (González et al., 2010).

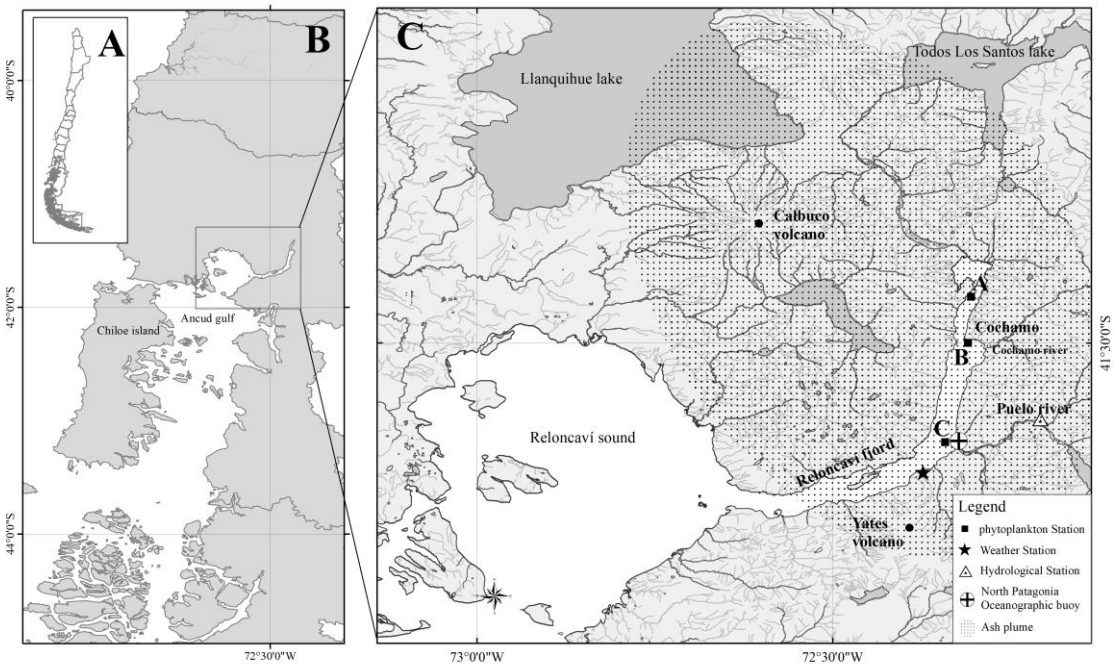

135

136 Figure 1. The Calbuco region showing the location of Reloncaví Fjord, 3 major rivers
137 (Petrohué, Cochamó and Puelo) discharging into the fjord, the 3 stations (black squares; A,
138 B and C) used to assess changes in phytoplankton abundance following the eruption, a
139 hydrological station that monitors Puelo river flow, a weather station and the location of a
140 long-term mooring within the fjord. The extent of the ash plume in the week following the
141 eruption is illustrated, as estimated in technical reports issued by the Servicio Nacional de
142 Geología y Minería.

143

144 On 22 April 2015 the Calbuco volcano erupted after 54 years of dormancy. Two major
145 eruption pulses lasted <2 hours on 22 April and 6 hours on 23 April, releasing a total volume
146 of 0.27 km^3 ash which was projected up to 20 km height above sea level (Van Eaton et al.,
147 2016; Romero et al., 2016). Ash layers of several cm thick were deposited mainly to the NE

of the volcano in subsequent days (Romero et al., 2016). Fortuitously, as part of a long-term deployment, an ocean acidification buoy in the middle of Reloncaví Fjord (Vergara-Jara et al., 2019) and an associated meteorological station close to the volcano (Fig. 1) were well placed to assess the impact of ash fall immediately after the eruption. To compliment data from these facilities, after the regional evacuation order was removed, weekly sampling campaigns were conducted in the fjord commencing one week after the eruption. The Chilean Geological-mining Survey (Servicio Nacional de Geología y Minería, SERNAGEOMIN) produced daily technical reports including the estimated area of ash dispersion (http://sitiohistorico.sernageomin.cl/volcan.php?pagina=4&iId=3). This information was used to create a reference aerial extent of ash deposition for the week after the eruption (Fig. 1, C).

2.2. Ash samples – trace metal leaching experiments

Ash (500 g) was collected (6 May 2015, in Cochamó, Chile) using a plastic tray wrapped with plastic sheeting (40 × 94 cm), double sealed in low density polyethylene (LDPE) plastic bags and stored in the dark. Ambient weather in the day preceding ash collection was dry. A sub-sample was analyzed for particle size using a Mastersizer 2000 at The University of Chile. Offshore seawater for incubation experiments was collected in the mid-South Atlantic (40° S) using a towfish and trace metal clean tubing in a 1 m^3 high density polyethylene tank which had been pre-rinsed with 1 M HCl. This water was stored in the dark for >12 months prior to use in leaching experiments. All labware for trace metal leaching experiments was pre-cleaned with Mucasol and 1 M HCl. 125 ml LDPE bottles (Nalgene) for trace metal leach experiments were pre-cleaned using a 3-stage procedure with three de-ionized water (Milli-

171 Q, Millipore, conductivity 18.2 MΩ cm^{-1}) rinses after each stage (3 days in Mucasol, 1 week
172 in 1 M HCl, 1 week in 1 M HNO_3).

173 Leach experiments were conducted by adding a pre-weighed mass of ash into 100 ml South
174 Atlantic Seawater, gently mixing the suspension for 10 minutes, and then syringe filtering
175 the suspension (0.2 µm, polyvinylidene fluoride, Millipore). Eight different ash loadings
176 from 2-50 mg L^{-1} were used, with each treatment run in triplicate. Samples for dissolved trace
177 metals (Fe, Cd, Pb, Ni, Cu, Co and Mn) were acidified within 1 day of collection by the
178 addition of 140 µL HCl (UPA grade, ROMIL) and analysed by inductively coupled plasma
179 mass spectroscopy following preconcentration exactly as per Rapp et al., (2017).

180 Leach experiments specifically to measure Fe(II) release were conducted in a similar manner
181 but in cold seawater due to the rapid oxidation rate of Fe(II) at room temperature (~21°C),
182 which makes accurate measurement of Fe(II) concentrations challenging (Millero et al.,
183 1987). A pre-weighed mass of ash was added to 250 ml South Atlantic seawater and manually
184 shaken for approximately one minute. Ash loadings ranged from 0.2-4000 mg L^{-1}. Fe(II) was
185 measured via flow injection analysis using luminol chemiluminescence (Jones et al., 2013)
186 without pre-concentration or filtration. The inflow line feeding the flow injection apparatus
187 was positioned inside the ash suspension immediately after mixing and measurements begun
188 thereafter at 2 minutes resolution. Reported mean values (± standard deviation) are
189 determined from the Fe(II) concentrations measured 2-30 minutes after adding ash into
190 solution. Calibrations were run daily using standard additions of 0.2-10 nM Fe(II) to aged
191 (unfiltered) South Atlantic seawater at the same temperature with integrated peak area used
192 to construct calibration curves. Following each leaching experiment the apparatus was rinsed
193 with 0.1 M HCl (reagent grade) followed by flushing with de-ionized water to ensure the

194 removal of ash particles. Blank measurements before/after Fe(II) measurements from
195 experiments with different ash loadings verified that there was no discernable interference
196 from ash particles in the Fe(II) flow through measurements. Fe(II) leaches were conducted 2
197 weeks, 4 months and 9 months after the eruption. The trace metal leach experiments (above)
198 were conducted at the same time as the first Fe(II) incubation experiments (2 weeks after ash
199 collection).

200 For trace metal leaches, the initial (mean ± standard deviation) dissolved trace metal
201 concentrations were deducted from the final concentrations, in order to calculate the net
202 change as a result of ash addition. For Fe(II) measurements, background levels of Fe(II) were
203 below detection (<0.1 nM) and so no deduction was made.

204 **2.3 Ash samples – de-ionized and brackish water leaching experiments**

205 Fresh brackish sub-surface water from the Patagonia study region was obtained from the
206 Aysén Fjord, at Ensenada Baja (45º21'S: 72º40'W, salinity 16.3), close to the Coyhaique
207 laboratory (Aysén region, Chile) and free from the influence of ash from the 2015 eruption.
208 The oceanographic conditions in these waters are similar to the adjacent Reloncaví fjord
209 (Cáceres et al., 2002; González et al., 2011). De-ionized water, along with the Aysén fjord
210 brackish water, were used for leaching experiments following recommendations of Witham
211 et al., (2005). Leaches were conducted in 50 ml LDPE bottles filled with either 40 ml brackish
212 or DI-water with 4 replicates of each treatment. Bottles were incubated inside a mixer at
213 room temperature after the addition of 0.18 g ash, using two ash size fractions (<63 μm and
214 250-1000 μm) which were separated using sieves (ASTM e-11 specification, W.S. Tyler).
215 The size distribution of the ash as determined by sieving was 4.54% >2360 μm; 6.85% <

2360 µm and >1000 µm; 31.12% <1000 µm and >250 µm; 24.14% <250 µm and >125 µm; 18.04% <125 µm and >63 µm; 15.31% <63 µm.

The sampling times were at time zero (defined as just after the addition of the ash and a few minutes of mixing), 2 h and 24 h later. Leaching experiments conducted with brackish water were analyzed for total alkalinity (A_T) via a potentiometric titration using reference standards (Haraldsson et al., 1997) ensuring a reproducibility of < 2 µmol/kg. For the de-ionized water leaching experiment, A_T was analyzed by titration of unfiltered 5 ml subsamples to a pH 4.5 endpoint (Bromocresol Green/Methyl Red) using a Dosimat (Metrohm Inc) and 0.02 N H_2SO_4 titrant. Alkalinity was calculated as $CaCO_3$ equivalents following APHA (American Public Health Association) 2005-Methods 2320 (2320 Alkalinity, titration method). Additional 5 ml subsamples were filtered, stored at 4°C and analyzed within 3 days for major ions (Fl^-, Cl^-, SO_4^{2-}, NO_3^-, Li^+, Na^+, NH_4^+, K^+, Mg^{2+}, Ca^{2+}) using a DionexTM 5000 Ion Chromatography system with Eluent Generation (APHA). All measurements were then corrected for initial water concentrations prior to ash addition.

Table 1. Summary of different leaching experiments and samples.

Ash/ particle source	Experiment type-objective	Nº of replicates
Calbuco Volcano ash, sieved <63 µm	Total alkalinity, brackish water	4
Calbuco Volcano ash, sieved <63 µm	Total alkalinity, ion and nutrient leaching, DI water	4
Calbuco Volcano ash, sieved 250-1000 µm	Total alkalinity, brackish water	4
Calbuco Volcano ash, sieved 250-1000 µm	Total alkalinity, ion and nutrient leaching, DI water	4
Calbuco Volcanic ash, unsieved	Trace metal leaches, S Atlantic seawater	3

Calbuco Volcanic ash, unsieved	Fe(II) leaches, chilled S Atlantic seawater	1*

*1 time series of >10 measurements at 2-minute intervals following ash addition into seawater. DI, de-ionized water.

2.4 Environmental data – continuous Reloncaví Fjord monitoring

High temporal resolution (hourly) in situ measurements were taken simultaneously in the Reloncaví fjord (Fig. 1 C, North Patagonia Oceanographic Buoy) at the surface and at 3 m depth for pCO_2, pH, depth, temperature, conductivity and dissolved O_2 using two SAMI sensors that measured spectrophotometric CO_2 and pH (DeGrandpre et al., 1995; Seidel et al., 2008) (Sunburst Sensors, LLC), and an SBE 37 MicroCAT CTD-ODO (SeaBird Electronics) for temperature, conductivity, depth and dissolved O_2, as per Vergara-Jara et al., (2019). Sensor maintenance and quality control is described by Vergara-Jara et al., (2019). The error in pCO_2 concentrations is estimated to be at most 5% which arises mainly due to a non-linear sensor response and reduced sensitivity at high pCO_2 levels >1500 ppm (DeGrandpre et al., 1999). The SAMI-pH instruments used an accuracy test instead of a calibration procedure (Seidel et al., 2008). With the broad pH and salinity range found in the fjord, pH values are subject to a maximum error of ±0.02 (Mosley et al., 2004).

A meteorological station (HOBO-U30, Fig. 1) measured air temperature, solar radiation, wind speed and direction, rainfall, and barometric pressure every 5 minutes. Puelo River streamflow was obtained from the Carrera Basilio hydrological station (Fig. 1), run by Dirección General de Aguas de Chile (http://snia.dga.cl/BNAConsultas/reportes).

2.5 Field surveys in Reloncaví Fjord post eruption

During May 2015, weekly field campaigns were undertaken in the Reloncaví Fjord. Phytoplankton samples were collected at 3 depths (1 m, 5 m and 10 m) for taxonomic characterization and abundance determination at 3 stations (A, B and C; Fig. 1) using a 5 L Go-Flo bottle. Samples were analyzed using a Olympus CKX41 inverted phase contrast microscope using a 10 ml sedimentation chamber and the Utermöhl method (Utermöhl, 1958). The phytoplankton community composition was then statistically analyzed in R (RStudio V 1.2.5033) using general linear models in order to find statistically significant differences between dates and group abundances. Additionally, as part of a long-term monitoring program at station C (Fig. 1), on 6 occasions during March-May 2015, chlorophyll-a samples were retained from 6 depths (1, 3, 5, 7, 10 and 15 m). Chlorophyll-a was determined after filtering 250 ml of sampled water through GFF filters (Whatman) by fluorometry as per Welschmeyer (1994). Two additional profiles close to Station C were obtained from Yevenes et al., (2019). Integrated chlorophyll-a (mg m^{-2}) and diatom abundance (cells m^{-2}) were determined to 15 m depth. Chlorophyll-a within Reloncaví Fjord is invariably concentrated in the upper ~10 m (González et al., 2010; Yevenes et al., 2019) and thus, for comparison to prior data reported integrated to 10 m, only a small difference is anticipated. For all profiles considered herein (Fig. 4), there is a 20% difference between integrating to 10 m or 15 m depth.

2.6 Satellite data

Daily, 4 km resolution chlorophyll-a images from the MODIS Aqua sensor (OCI algorithm; Hu et al., 2012) were downloaded from the NASA Ocean Color website (https://oceancolor.gsfc.nasa.gov) for the period 4 April 2015–2 May 2015. As a proxy for the spatial extent and loading of the ash plume, the UV aerosol index product from the Ozone

Monitoring Instrument (OMI) on the EOS-Aura was downloaded for the same time period. Daily images were composited into 5-day mean averages (Fig. 7).

3. Results

3.1 In situ observations

The Calbuco ash plume reached up to 20 km height and was dispersed hundreds of kilometers across Patagonia and the Pacific and Atlantic Oceans (Fig. 2) (Eaton et al., 2016; Romero et al., 2016; Reckziegel et al., 2016). The ash loading in water bodies near the cone was visually observed to be high, especially near the Petrohué river catchment that drains into the head of the Reloncaví fjord. This ash loading into the fjord was clearly visible on 6 May 2015 when ash samples were collected for leaching experiments (Fig. 2).

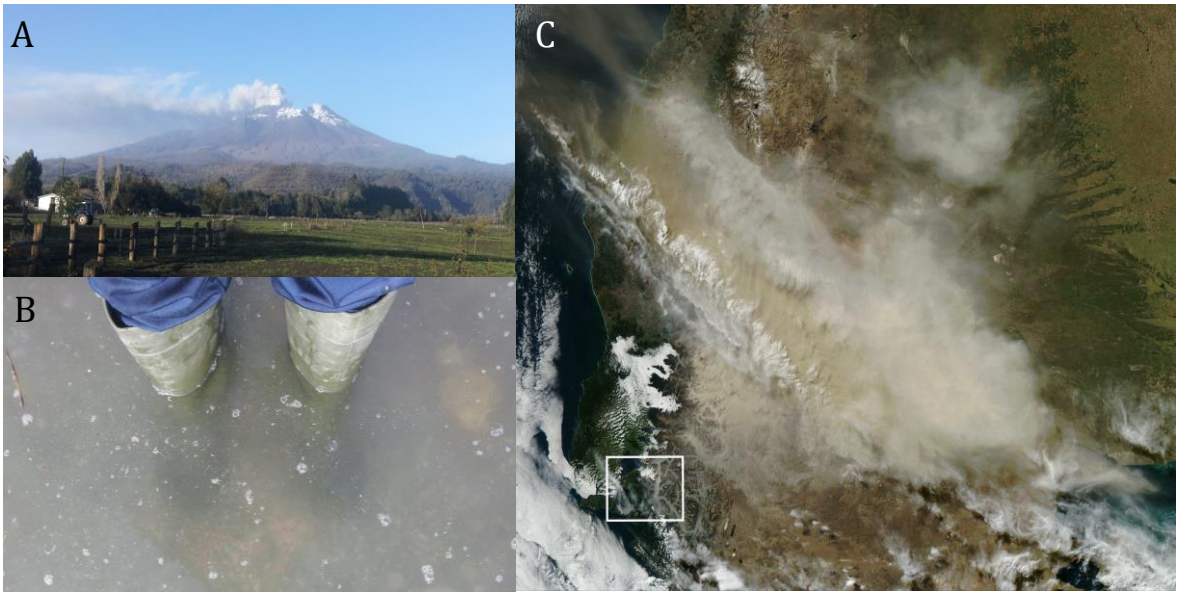

Figure 2. A Calbuco volcano ash plume May 6 2015. B Reloncaví Fjord water with atypical high turbidity due to the ash loading, Cochamó town 6 May 2015. C Ash cloud visible on MODIS Aqua satellite from the NASA Earth Observatory, April 23

(http://earthobservatory.nasa.gov/NaturalHazards/view.php?id=85767&eocn=home&eoci=nh). The highlighted box in C corresponds to Fig. 1 C.

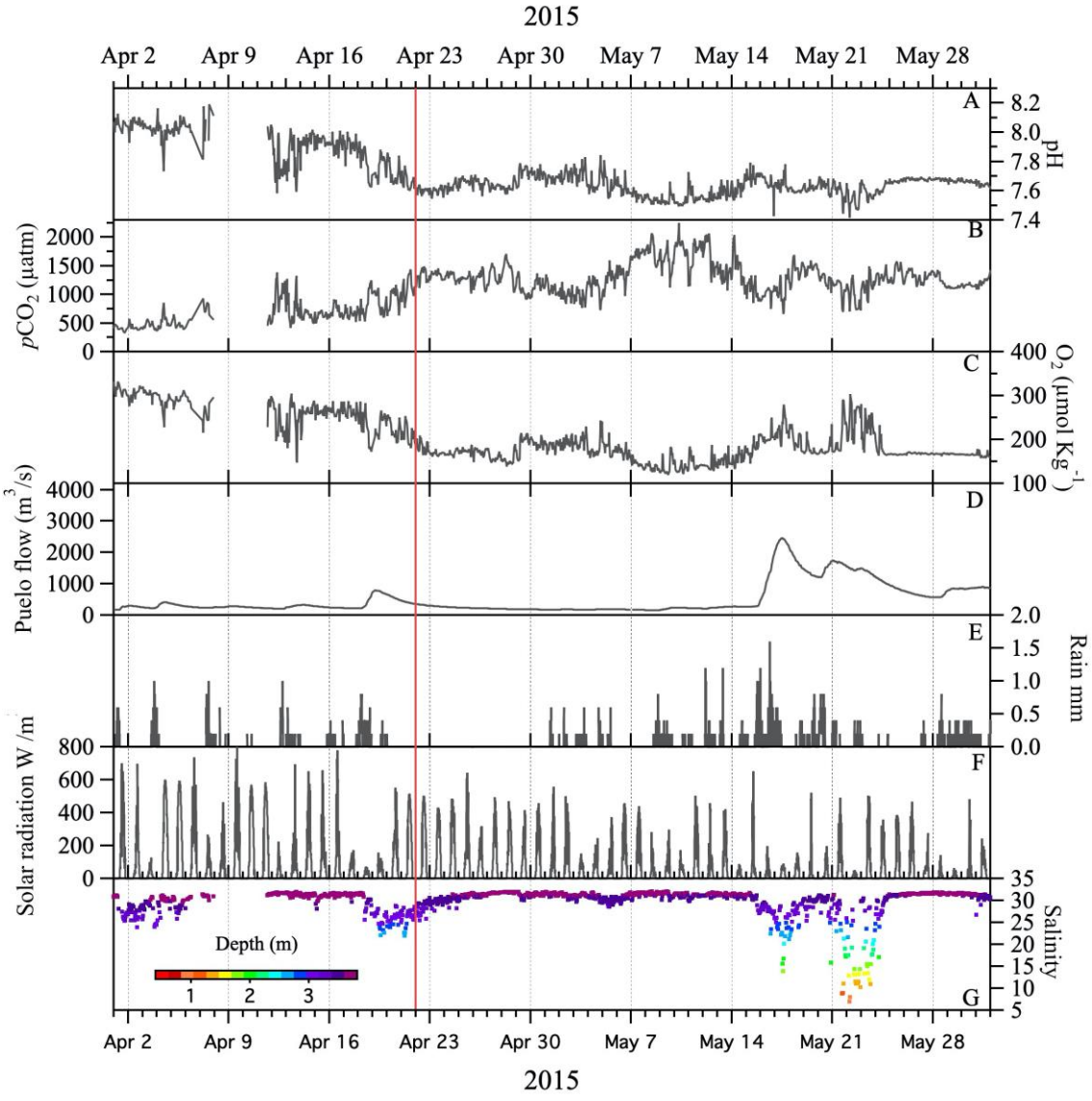

Figure 3. Continuous data from the Reloncaví Fjord mooring and nearby hydrological and weather stations for April-May 2015. The vertical red line marks the eruption date. All locations are marked in Fig 1. Carbonate chemistry and salinity data from Vergara-Jara et al., (2019). Wind and tidal mixing caused small changes in the depth of the sensors which are shown alongside the salinity data.

Carbonate chemistry data from the Reloncaví Fjord mooring demonstrated that pH declined and pCO_2 increased in the week prior to the eruption (22 April, Fig. 3). Oxygen and pH reached a minimum and pCO_2 a maximum during the time period May 7-14, which indicates a state of high respiration. In this stratified environment, the brackish fjord surface layer has generally low pH, high pCO_2 with seasonal changes in salinity and respiration leading to a large annual range of pCO_2 and pH (Vergara-Jara et al., 2019). The depth of the sensors varied temporally due to changes in tides and river flow. This accounts for some of the variation in measured salinity due to the strong salinity gradient with depth in the brackish surface waters (Fig. 3). Any changes to pCO_2 or pH occurring as a direct result of the eruption, or associated ash deposition, are therefore challenging to distinguish from background variation due to short-term (intra-day) or seasonal shifts in the carbonate system which are pronounced in this dynamic and strongly freshwater influenced environment (Fig. 3). Freshwater discharge from the Puelo increased sharply from May 16 which is an annually recurring event (González et al., 2010).

3.2 Phytoplankton in Reloncaví fjord post-eruption

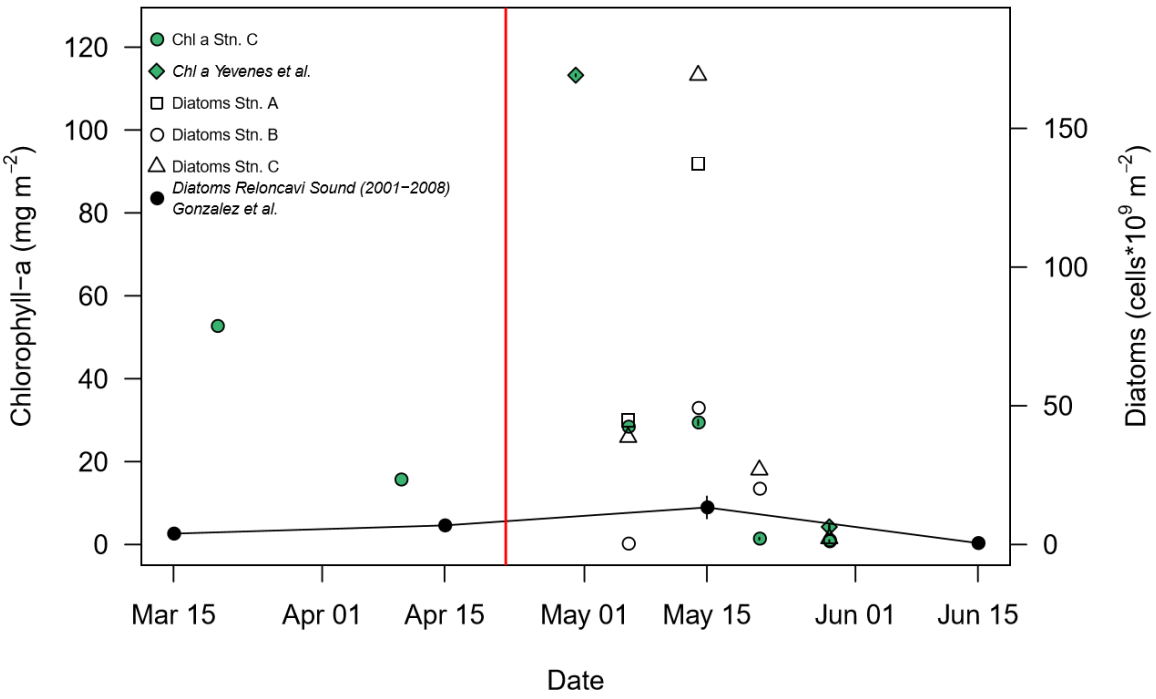

312

313 Figure 4. Changes in integrated (0-15 m) diatom abundance and chlorophyll-a for Reloncaví
314 Fjord in April-May 2015. Locations as per Fig. 1, the eruption date (22 April) is marked with
315 a red line. Historical diatom data from Reloncaví Sound (2001-2008, integrated to 10 m
316 depth, mean ± standard error, González et al., 2010) and additional chlorophyll data from
317 2015 ('Station 3' from Yevenes et al., 2019, approximately corresponding to Station C
318 herein) are also shown.

319

320 Phytoplankton abundances observed in May 2015 within Reloncaví Fjord were assessed by
321 diatom cell counts and chlorophyll-a concentrations and were proportionate to, or higher
322 than, those previously observed in the region (Fig. 4). When comparing observations to prior
323 data from González et al., (2010) it should be noted that there is a slight depth discrepancy
324 (earlier work was integrated to 10 m depth rather than 15 m herein). Yet as the phytoplankton
325 bloom is overwhelmingly present within the upper 10 m these data do provide a useful

comparison. Diatom abundance integrated to 15 m depth peaked at Stations A and C around 14th May, with notably lower abundances at the more freshwater influenced station B (Fig. 4), located at a mid-fjord site between the 3 major river outflows. The highest measured chlorophyll-a concentrations were on 30th April at Station C, including two nearby measurements from Yevenes et al., (2019), then chlorophyll-a values declined to much lower concentrations in late May which is expected from patterns in regional primary production (González et al., 2010). No measurements were available for 10-30 April 2015 (Fig. 4) and thus it is not possible to determine the timing of the onset of the austral autumn phytoplankton bloom with respect to the volcanic eruption from the available chlorophyll-a or diatom data. Within this time period, the mooring at Station C (Fig. 3) however did record a modest increase in pH and O_2 from 28-29 April, during a time period when river discharge and salinity were stable, which could be indicative of the autumn phytoplankton bloom onset.

3.3 Total alkalinity and macronutrients in leach experiments

Size analysis of the collected ash determined a mean particle diameter of 339 µm. Small ash-particles (<63 µm) resulted in minor, or no significant, changes to A_T in brackish fjord waters (Fig. 5). With large ash-particles (>1.0 mm) no effect was evident. Conversely, a leaching experiment with de-ionized water showed a small increase in A_T (Fig. 5) for both size fractions. By increasing the A_T of freshwater, ash would act to increase the buffering capacity of river outflow into a typically weak carbonate system like the Reloncaví Fjord (Vergara-Jara et al., 2019). However, the absolute change in A_T was relatively small despite the large ash loading used in all incubations (< 20 µmol kg^{-1} A_T for ash loading >4 g L^{-1}) and therefore it is expected that the direct effect of ash on A_T in situ was limited. Other effects on carbonate

chemistry may however arise due to ash moderating the timing and intensity of primary production and thus biological pCO_2 drawdown.

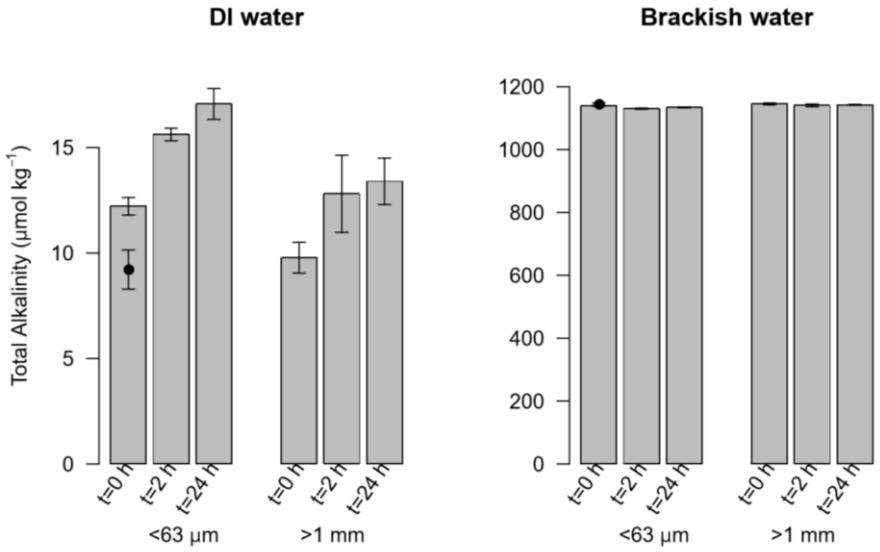

Figure 5. Total alkalinity released after leaching 4.5 g L^{-1} ash of two size fractions (<63 µm and >1.0 mm) in de-ionized water (DI water) and brackish water. T_0= 'time zero', measured after one minute of mixing, T_{2H}= after two hours of mixing, T_{24H}= after 24 hours of mixing. n=4 for all treatments (mean ± standard deviation plotted). The initial (pre-ash addition) alkalinity is marked by a black dot superimposed on the left T_0.

Ion chromatography results for Na, K, Ca, Fl, Cl, NO_3 and SO_4 showed that in the presence of smaller ash size particles, ion inputs were generally higher. The leaching from ash components into de-ionized water occurred almost instantly with limited, or no increases in leached concentrations observed between 0, 2 and 24 h (Table 2). For larger particles there was less release of most ions. In the case of Ca and SO_4 a more gradual leaching effect was apparent (Table 2). The concentrations of NO_3 and NH_4 were generally below detection suggesting that ash was a minor source of these nutrients into solution. These observations

are consistent with the trends in prior work using a range of volcanic ash and incubation conditions (Delmelle et al., 2007; Duggen et al., 2010; Witham et al., 2005).

	Time [h]	**Na^+**	**K^+**	**Ca^{2+}**	**Fl^-**	**Cl^-**	**SO_4^{2-}**	**NO_3^-**	**NH_4^+**
Detection limit		*0.17*	*0.43*	*0.30*	*0.28*	*1.31*	*1.64*	*0.34*	*0.13*
Proced. Blank		b.d.	b.d.	0.39	b.d.	b.d.	b.d.	b.d.	b.d.
>1.0 mm	0.1	3.4 (2.8)	0.83 (0.3)	18.3 (3.3)	0.16 (0.05)	3.7 (1.9)	3.7 (2.2)	b.d.	0.15 (0.2)
[µmol/l]	2	5.1 (2.0)	1.0 (0.2)	18.5 (4.5)	0.21 (0.08)	4.4 (1.6)	4.9 (2.0)	b.d.	0.38 (0.4)
	24	7.3 (0.1)	1.4 (0.2)	23.4 (3.2)	0.52 (0.18)	5.7 (0.5)	8.3 (2.1)	b.d.	b.d.
<63 µm	0.1	16.2 (12.7)	3.2 (0.3)	25.1 (5.4)	0.29 (0.0)	17.1 (13.6)	13.5 (1.3)	0.53 (0.2)	1.70 (1.1)
[µmol/l]	2	16.7 (1.0)	3.8 (0.1)	31.8 (2.7)	0.63 (0.2)	15.2 (0.9)	19.0 (0.3)	b.d.	0.52 (1.0)
	24	17.3 (0.8)	3.9 (0.3)	33.8 (3.3)	0.69 (0.3)	14.6 (1.0)	18.8 (0.5)	b.d.	1.32 (2.6)
<63 µm	24	3.84	0.87	7.50	0.15	3.25	4.18	0.048	0.29
[µmol/g ash]	Range (lit.)	1.5-84.3	0.1-5.4	0.6-589	0.1-9	2-92.9	1-554	0-6.4	0.3-0.6

Table 2. Major ion and macronutrient concentrations in µmol/l leached from the two size fractions of ash (< 63 µm and >1.0 mm) into deionized water (b.d. = below detection). Shown are mean, with standard deviation in parentheses (n=4). Also shown are mass normalized values [µmol/g ash], and a comparison to the range of values reported by Jones and Gislason, (2008).

3.4 Trace elements in leach experiments

Release of nanomolar concentrations of dissolved Fe and Mn was evident when ash was re-suspended in aged seawater for 10 minutes (Fig. 6). The net release of dissolved metals proceeded with varying relationships with ash loading over the applied gradient (0.1 - 6 mg L^{-1}). Dissolved Mn, Pb, Cu and Co release exhibited significant ($p < 0.05$) positive relationships with ash loading, with Mn and Cu exhibiting the most linear behavior (R^2 0.99 and 0.83, respectively). The initial concentration of metals in South Atlantic seawater should however also be considered when interpreting the trends. The magnitude of changes in Cd

and Ni concentrations were smallest relative to both the initial concentration and the standard deviation on the initial concentration (0.38 ± 0.04 nM Cd and 6.58 ± 0.76 nM Ni, respectively). It thus would be difficult to extract a clear relationship irrespective of their chemical behavior. For other elements, non-linearity between ash addition and trace metal concentrations, and some negative changes in concentrations, both likely reflect scavenging of metal ions onto ash particle surfaces (Rogan et al., 2016). Fe, Co and Pb are all scavenged type elements and so increasing the surface area of ash present may affect the net change in metal concentration.

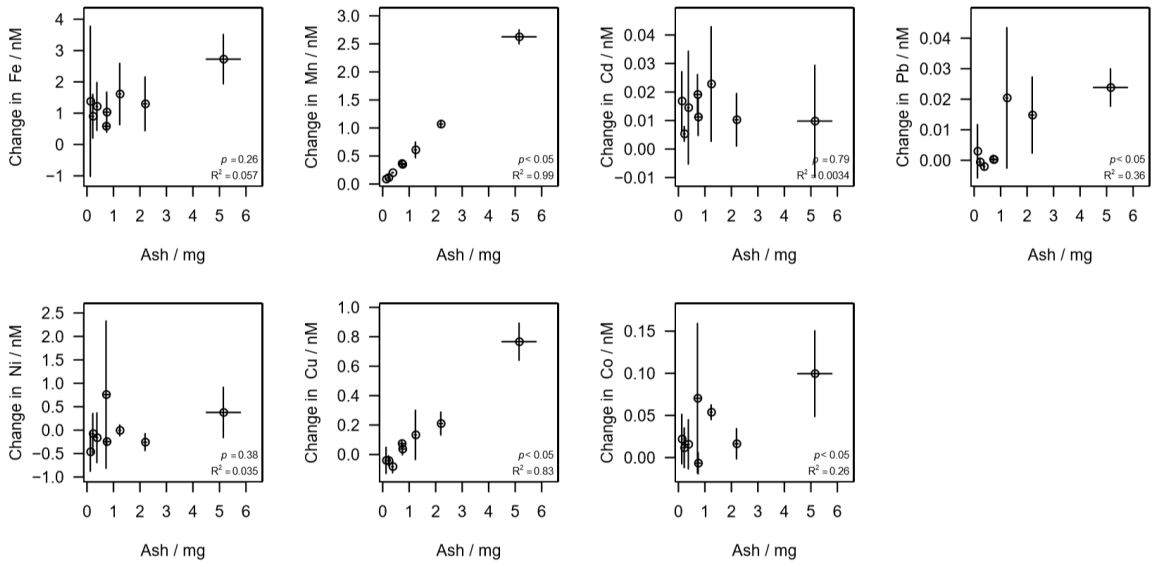

Figure 6. Change in trace metal concentrations after varying ash addition to 100 ml South Atlantic seawater for a 10-minute leach duration at room temperature. Initial (mean ± standard deviation) dissolved trace metal concentrations - deducted from the final concentrations to calculate the change as a result of ash addition - were 0.98 ± 0.03 nM Fe, 0.38 ± 0.04 nM Cd, 13 ± 2 pM Pb, 6.58 ± 0.76 nM Ni, 0.84 ± 0.07 nM Cu, 145 ± 9 pM Co, 0.72 ± 0.05 nM Mn. Error bars are standard deviations from triplicate treatments with similar ash loadings. p values and R^2 for a linear regression are annotated.

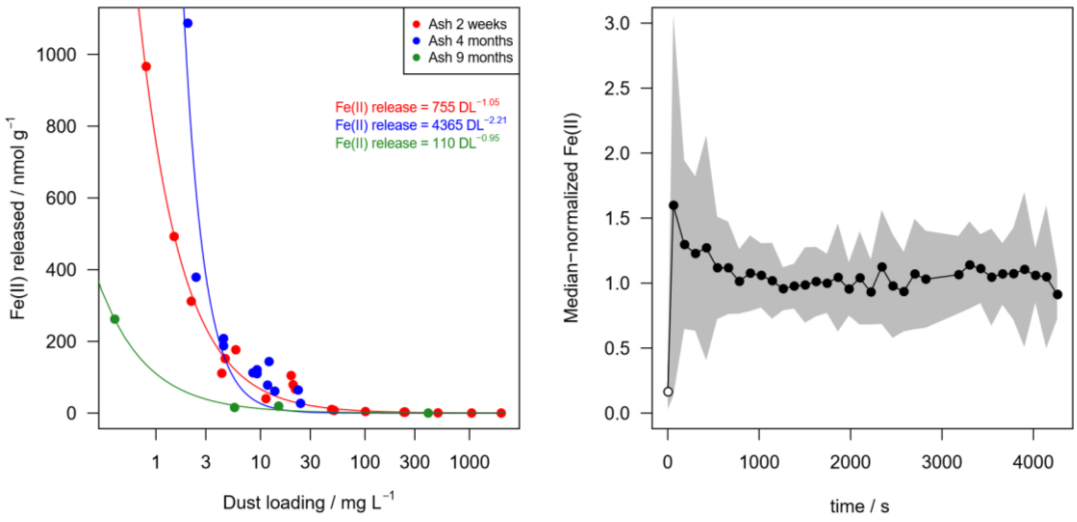

Figure 7. Fe(II) release from ash into seawater. Mean Fe(II) released into South Atlantic seawater over a 30 minute leach at 5-7°C (left). The same batch of Calbuco ash was subsampled and used to conduct experiments on 3 occasions after the 2015 eruption (2 weeks, 4 months and 9 months since ash collection). The 30 minute time-series of Fe(II) concentrations following ash addition are considered collectively by normalizing the measured concentrations (right), such that 1.0 represents the median Fe(II) concentration measured in each experiment 2-30 minutes after ash addition. The black line shows the mean response over 34 leach experiments with varying ash loading, the shaded area shows ± 1 standard deviation. The initial Fe(II) concentration (pre-ash addition at 0 s) in all cases was below detection and thus the detection limit is plotted at 0 s (open circle).

In addition to the release of dFe in solution, which generally exists as Fe(III) species in oxic seawater (Gledhill and Buck, 2012), the release of Fe(II) was evident on a similar timescale when cold (5-7°C) aged S Atlantic seawater was used as leachate (Fig. 7). The half-life of Fe(II) decreases more than tenfold as temperature is increased from 5 to 25°C, leading to Fe(II) decay on timescales shorter than the time required for analysis (approximately 60 s for

414 solution to enter the flow injection apparatus, mix with reagent and generate a peak)
415 (Santana-Casiano et al., 2005). Elevated concentrations of up to 4.0 nM Fe(II) were evident
416 at this temperature (5-7°C), which represents an intermediate sea surface temperature for the
417 high latitude ocean. A sharp decline in Fe(II) dissolution efficiency with increasing ash load
418 was also evident (Fig. 7). Both the highest Fe(II) concentration and the highest net release of
419 Fe(II) were observed at the lowest ash loading (Fig. 7). Fe(II) concentration following dust
420 addition into seawater was possibly reduced when the same experimental leaches with ash
421 were repeated 9 months after the initial experiment. The first leaches were conducted ~2
422 weeks after ash collection. The absence of a clear change between 2 weeks and 4 months
423 precludes an accurate assessment of the rate at which Fe(II) solubility may have decreased.
424 As Fe(II) concentrations were measured continuously using flow injection analysis, the
425 temporal development of Fe(II) concentration after ash addition to cold seawater can also be
426 shown (Fig. 7). Considering the set of leach experiments collectively, all ash additions were
427 characterized by a sharp increase in Fe(II) concentrations in the first minute after ash addition
428 into seawater. This was typically followed by a decline and then a relatively stable Fe(II)
429 concentration (Fig. 7).

430 **3.5 Satellite observations**

431 Five-day composite images of atmospheric aerosol loading (UV aerosol index) indicated two
432 main volcanic eruption plume trajectories: (i) northwards over the Pacific, and (ii) northeast
433 over the Atlantic. Daily resolved time series were constructed for regions in the Atlantic and
434 Pacific with elevated atmospheric aerosol loading (UV Aerosol Index ~2 a.u.; Fig. 8). The
435 Pacific time series indicated a pronounced peak in aerosol index followed by chlorophyll-a
436 one day later. A control region to the south of the ash-impacted Pacific region showed no

clear changes in chlorophyll-a matching that observed in the higher UV aerosol index region to the north.

Conversely in the Atlantic, where the background chlorophyll-a concentration was higher throughout the time period of interest, the main area with enhanced aerosol index was not clearly associated with a change in chlorophyll-a dynamics on a timescale comparable to that observed following other volcanic ash fertilized events (Fig. 8). In a smaller ash impacted area to the south of the Rio de la Plata (Sup. Fig. 3), where nitrate levels are expected to be higher than to the north and Fe levels also expected to be elevated due its location on the continental shelf, a chlorophyll-a peak was evident 7 days after the UV aerosol peak. However, this was not well constrained due to poor satellite coverage in the period after the eruption.

Prior eruptions have been attributed with driving time periods of enhanced regional marine primary production beginning 3-5 days post-eruption (Hamme et al., 2010; Langmann et al., 2010; Lin et al., 2011) and bottle experiments showing positive chlorophyll changes in response to ash addition are typically significant compared to controls within 1-4 days following ash addition (Browning et al., 2014; Duggen et al., 2007; Mélançon et al., 2014).

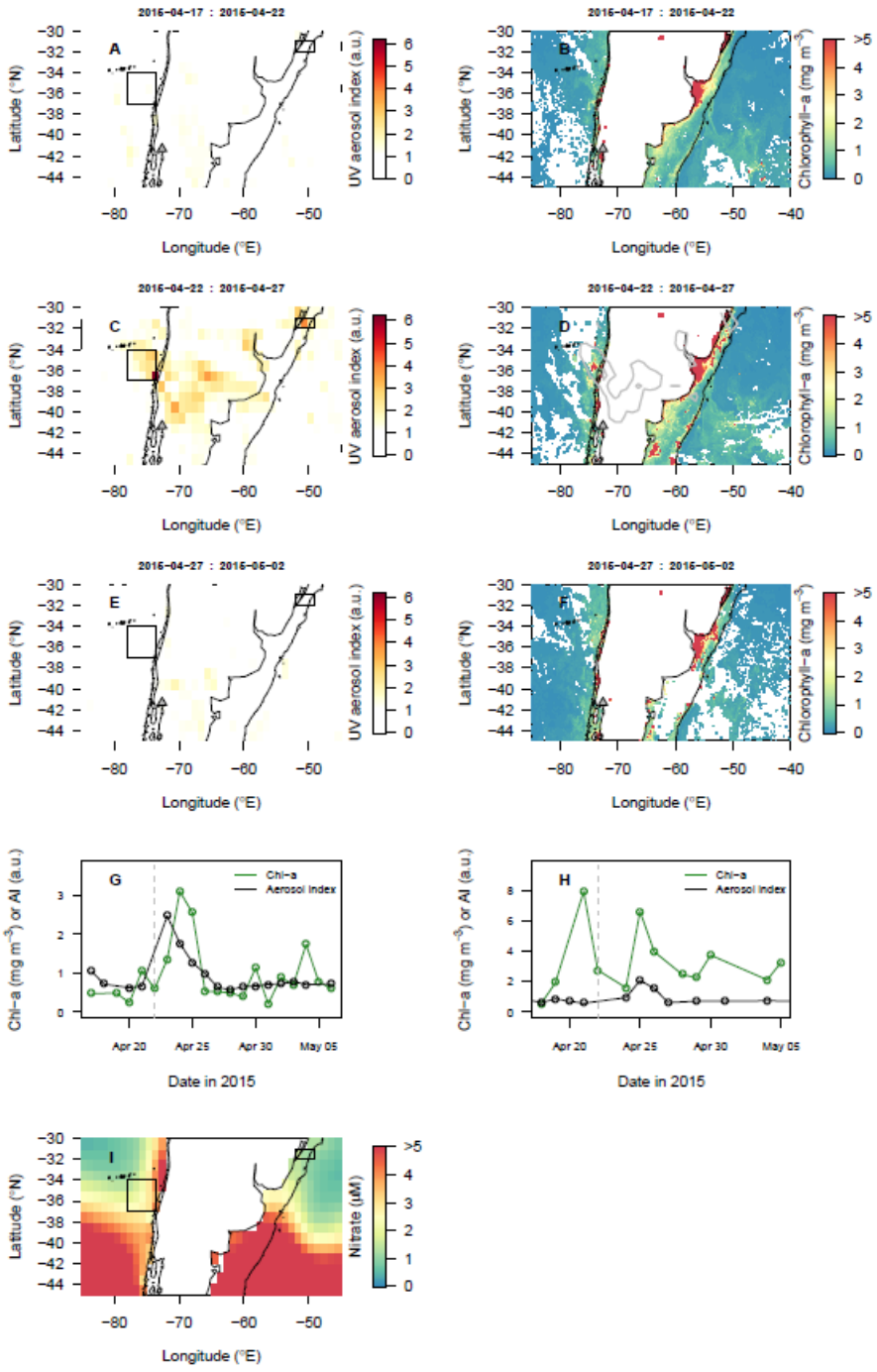

453

454 Figure 8. Potential biological impact of the 2015 Calbuco eruption observed via satellite
455 remote sensing. (A-F) Spatial maps showing the distribution of ash in the atmosphere (UV
456 Aerosol Index) and corresponding images of chlorophyll-a. Images were composited over 5-
457 day periods. Grey lines in chlorophyll maps corresponds to the UV Aerosol index = 2 a.u.

contour. (G, H) Time series of UV Aerosol Index and chlorophyll-a for regions of the Pacific (G) and Atlantic (H) identified by boxes in maps. Dashed vertical lines (22 April) indicate the eruption date. (I) Mean World Ocean Atlas surface NO_3 concentrations. Thin black lines indicate the 500 m bathymetric depth contour.

4 Discussion

4.1 Local drivers of 2015 bloom dynamics in Reloncaví Fjord

The north Patagonian archipelago and fjord region have a seasonal phytoplankton bloom cycle with peaks in productivity occurring in May and October (austral autumn and spring) and the lowest productivity consistently in June (austral winter) (González et al., 2010). Diatoms normally dominate the phytoplankton community during the productive period due to high light availability and high silicic acid supply, both of which are influenced by freshwater runoff (González et al., 2010; Torres et al., 2014). The austral fall season, encompassing the April-May 2015 ash fall, is therefore expected to have a high phytoplankton biomass (Iriarte et al., 2007; León-Muñoz et al., 2018) which terminates abruptly with decreasing light availability in austral winter (González et al., 2010).

Whilst not directly comparable, the magnitude of the 2015 bloom in terms of diatom abundance (Fig. 4) was more intense than that reported in Reloncaví Sound 2001-2008. With respect to the timing of the phytoplankton bloom, the low diatom abundances and chlorophyll-a concentrations at the end of May (Fig. 4) are consistent with prior observations of sharp declines in primary production moving into June (González et al., 2010). Peaks in diatom abundance were measured at two stations on 14th May, and measured chlorophyll-a concentrations were highest close to Station C on 30 April (Fig. 4). The high-resolution pH

and O_2 data collected at Station C from mooring data is consistent with an intense phytoplankton bloom between ~29 April and 7 May (Fig. 3) indicated by a shift to slightly higher pH and O_2 during this time period when river flow into the fjord was stable.

Without a direct measure of ash deposition per unit area in the fjord, turbidity, or higher resolution chlorophyll/diatom data, it is challenging to unambiguously determine the extent to which the austral autumn phytoplankton bloom was affected by volcanic activity. The high abundance of diatoms at two of three stations sampled could have resulted from ash fertilization. Yet if this was the case, it is not clear which nutrient was responsible for this fertilization, why the bloom initiation occurred several weeks after the eruption, and to what extent the timing was coincidental given that productivity normally peaks in May. Reloncaví Fjord was to the south of the dominant ash deposition (Romero et al., 2016). Both runoff and rainfall were vectors by which ash was deposited in the fjord, which complicates the interpretation of the time series provided by high resolution data (Fig. 3). With incident light also highly variable over the time series (Fig. 3F), there are clearly several factors, other than volcanic ash deposition, which will have exerted some influence on diatom and chlorophyll-a abundance throughout May 2015.

Primary production in the Reloncaví region is thought to be limited by light availability rather than macronutrient availability (González et al., 2010). Whilst micronutrient availability relative to phytoplankton demand has not been extensively assessed in this fjord, with such higher riverine inputs across the region- which are normally a large source of dissolved trace elements into coastal waters (e.g. Boyle et al., 1977)- limitation of phytoplankton growth by Fe, or another micronutrient, seems implausible. Reported Fe concentrations determined by

a diffusive gel technique in Reloncaví Fjord in October 2006 were relatively high; 46-530 nM (Ahumada et al., 2011). Similarly, reported dFe concentrations in the adjacent Comau Fjord at higher salinity are generally in the nanomolar range and remain >2 nM even under post-bloom conditions which suggests dFe is not a limiting factor for phytoplankton growth (Hopwood et al., 2020; Sanchez et al., 2019).

Silicic acid availability could have been increased by ash deposition. Whilst not quantified herein, an increase in silicic acid availability from ash in a region where silicic acid was sub-optimal for diatom growth could plausibly explain higher than usual diatom abundance (Siringan et al., 2018). Silicic acid concentrations were indeed high (up to 80 µM) in Reloncaví Fjord surface waters in May 2015 (Yevenes et al., 2019), however concentrations in excess of 30 µM are typical during periods of high runoff and accordingly are not thought to limit primary production or diatom growth (González et al., 2010). The $Si(OH)_4$:NO_3 ratio in Reloncaví Fjord and downstream Reloncaví Sound also indicates an excess of Si, with ratios of approximately 2:1 observed in fjord surface waters throughout the year (González et al., 2010; Yevenes et al., 2019). For comparison, the ratio of Si:N for diatom nutrient uptake is 15:16 (Brzezinski, 1985). Furthermore, experimental incubations making additions of macronutrients to fjord waters in Reloncaví and adjacent fjords, have found strong responses of phytoplankton to additions of silicic acid only when $Si(OH)_4$ and NO_3 were added in combination, further corroborating the hypothesis that an excess of silicic acid is normally present in surface waters of these fjord systems (Labbé-Ibáñez et al., 2015). It is therefore doubtful that changes in nutrient availability from ash alone could explain such high diatom abundances in mid-May.

530 Alternative reasons for high diatom abundances in the absence of a chemical fertilization
531 effect are plausible and could include, for example, ash having reduced zooplankton
532 abundance or virus activity in the fjord, thus facilitating higher diatom abundance than would
533 otherwise have been observed by decreasing diatom mortality rates in an environment where
534 nutrients were replete. The role of volcanic ash in driving such short-term ecological shifts
535 in the marine environment is almost entirely unstudied (Weinbauer et al., 2017). However,
536 volcanic ash deposition of 7 mg L^{-1} in lakes within this region during the 2011 Puyehue-
537 Cordón Caulle eruption was reported to increase post-deposition phytoplankton biomass and
538 decrease copepod and cladoceran biomass (Wolinski et al., 2013). The proposed mechanism
539 was ash particle ingestion negatively affecting zooplankton and ash-shading positively
540 affecting phytoplankton via reduced photoinhibition (Balseiro et al., 2014; Wolinski et al.,
541 2013).
542
543 Considering the more modest peak in diatom abundance at the most strongly ash affected
544 station (Station A, Fig. 4) and the timing of the peak diatom abundance 3 weeks after the
545 eruption, it is clear that the interaction between ash and phytoplankton in the Reloncaví Fjord
546 was more complex than the simple Fe-fertilization proposed for the SE Pacific (Fig. 8g). In
547 the absence of an immediate diatom fertilization effect from Fe or silicic acid, we hypothesize
548 that any change in phytoplankton bloom dynamics within Reloncaví Fjord was mainly a 'top-
549 down' effect driven by the physical interaction of ash and different ecological groups in a
550 nutrient replete environment, rather than a 'bottom-up' effect driven by alleviation of
551 nutrient-limitation from ash dissolution.
552 **4.2 Volcanic ash as a unique source of trace elements**

553 The release of the bioessential elements Fe and Mn from ash here ranged from 53 - 1200
554 nmol g^{-1} (dFe) and 48 - 71 nmol g^{-1} (dissolved Mn), which is comparable to the rates
555 determined in other studies under similar experimental conditions (Duggen et al., 2010).
556 Fe(II) release was particularly efficient at ash loadings <5 mg L^{-1} (Fig. 7) whereas dFe release
557 was less sensitive to ash loading (Fig. 6). The timing of Fe(II) release in the first 60 s of
558 incubations suggests a fast dissolution process. Fe(II) is short lived in oxic surface seawater
559 with an observed half-life of only 10-20 minutes even in the Southern Ocean where cold
560 surface waters slow Fe(II) oxidation (Sarthou et al., 2011). Yet, relative to Fe(III), Fe(II) is
561 also more soluble and, from an energetic perspective, expected to be more bioaccessible to
562 cellular uptake (Sunda et al., 2001). Whilst it is known that the vast majority of dFe leached
563 from ash into seawater tends to occur in the first minutes of ash addition (Duggen et al., 2007;
564 Jones and Gislason, 2008) and this could be consistent with rapid dissolution of highly
565 soluble phases on ash surfaces, we note that there is not yet conclusive evidence concerning
566 the precise origin of this dFe pulse. Fe(II) salts may be present on the surface of ash particles
567 (Horwell et al., 2003; Hoshyaripour et al., 2015) and thus the Fe(II) observed herein (Fig. 7)
568 may reflect almost instantaneous release following dissolution of thin layers of salt coatings
569 in ash surfaces (Ayris and Delmelle, 2012; Delmelle et al., 2007; Olsson et al., 2013).
570 Alternatively Fe(II) could be released from more crystalline Fe(II) phases. Prior work, at
571 much lower pH (pH 1 H_2SO_4 representing conditions that ash surfaces may experience during
572 atmospheric processing) suggests that short-term release of Fe(II) or Fe(III) is determined by
573 the surface Fe(II)/Fe ratio which may differ from the bulk Fe(II)/Fe ratio due to plume
574 processing (Maters et al., 2017).
575 Different leaching protocols are widely recognised as a major challenge for interpreting and
576 comparing different dissolution experiment datasets for all types of aerosols (Duggen et al.,

2010; Morton et al., 2013). When Fe(II) is released into solution as a considerable fraction of the total dFe release this is particularly challenging to monitor, as Fe(II) oxidises on timescales of seconds to minutes depending on temperature, pH and O_2 conditions (Santana-Casiano et al., 2005). The dFe and Fe(II) leaching protocols used herein are only comparable qualitatively, as the Fe(II) method using cooler seawater and larger seawater volumes was specifically designed to test for the presence of rapid Fe(II) release and to evaluate the short-term temporal trend of any such release. Yet, for rough comparative purposes, the Fe(II) released was equivalent to 38 ± 25% (mean ± standard deviation) of dFe released at ash loadings from 1-10 mg L^{-1} and 19 ± 17% of dFe for ash loadings from 10-50 mg L^{-1}. These values are reasonably comparable to the 26% median Fe(II)/dFe fraction measured in Fe released into seawater from aerosols collected across zonal transects of the Pacific Ocean (Buck et al., 2013) suggesting that fresh Calbuco ash is roughly comparable in terms of Fe(II) lability to these environmentally processed aerosols.

4.3 A potential fertilization effect in the SE Pacific

Experiments with ash suspensions have shown that ash loading has a restricted impact on satellite chlorophyll-a retrieval (Browning et al., 2015), therefore offering a means to assess the potential biological impact of the 2015 Calbuco eruption in offshore waters. We found evidence for fertilization of offshore Pacific seawaters in the studied area (Fig. 8). Following the eruption date, mean chlorophyll-a concentrations increased ~2.5 times over a broad region where elevated UV aerosol index was detected (Fig. 8G). Both the timing and location of this chlorophyll-a peak were consistent with ash fertilization, with the peak of elevated chlorophyll-a being located within the core of highest atmospheric aerosol loading, and the peak date occurring one day after the main passage of the atmospheric aerosol plume. A similar phytoplankton response timeframe was reported following ash deposition in the NE

Pacific following the August 2008 Kasatochi eruption (Hamme et al., 2010) which was similarly thought to be triggered by relief of Fe-limitation (Langmann et al., 2010). At the same time, a control region to the south of the ash-impacted Pacific region showed no clear changes in chlorophyll-a matching that observed in the higher UV aerosol index region to the north (Sup. Fig. 3).

A smaller ash impacted area to the south of the Rio de la Plata, where nitrate levels are expected to be higher than to the north, but with Fe levels also expected to be elevated due its location on the continental shelf, showed a chlorophyll-a peak 7 days after the UV aerosol peak (Sup. Fig. 3). However, this was not well constrained due to poor satellite coverage in the period after the eruption. Considering the dynamic spatial and temporal variation in chlorophyll within this coastal area, it is challenging to associate any change in chlorophyll specifically with ash arrival.

The change in chlorophyll-a observed in the SE Pacific contrasts with results in Reloncaví Fjord where phytoplankton abundances likely peaked much later than the first ash arrival-after 28 April. The fertilized region of the Pacific (Fig. 8) hosts upwelling of deep waters, supplying nutrients in ratios that are deficient in dFe (Bonnet et al., 2008; Torres and Ampuero, 2009). Fe-limitation of phytoplankton growth in this region is therefore anticipated, which could have been temporarily relieved following ash deposition and dFe release (Fig. 6). Conversely, ash deposition into the south western Atlantic indicated by the UV aerosol index did not lead to such a clear corresponding change in chlorophyll-a concentrations (Fig. 8H), although with the available data it is not possible to rule out the possibility of fertilisation completely (e.g., whilst also being proceeded by a larger chlorophyll-a peak on August 21st, there is a peak in chlorophyll-a at August 25th coinciding

with elevated UV aerosol index). Phytoplankton growth in this region of the Atlantic is expected to be limited by fixed nitrogen availability, as a result of strong stratification (Moore et al., 2013) and thus dFe release from ash particles would not be expected to result in short-term increases to primary production. The differential responses observed in the Pacific and Atlantic are therefore consistent with the anticipated nutrient limitation regimes (Fe-limited and nitrogen-limited, respectively), and the supply of dFe but not fixed N (NO_3 or NH_4) from the Calbuco ash (Fig. 6 and Table 2).

5 Conclusions

The contrasting effects of volcanic ash on primary producers in Reloncaví Fjord, the SE Pacific and SW Atlantic Oceans support the hypothesis that the response of primary producers is dependent on both the ash loading and the resources limiting primary production in a region at a specific time of year. Leach experiments using ash from the 2015 Calbuco eruption demonstrated a small increase in the alkalinity of de-ionized water from fine, but not coarse ash, and no significant addition of fixed nitrogen (quantified as NO_3 and NH_4) into solution. In saline waters, release of dissolved trace metals including Mn, Cu, Co, Pb, Fe and specifically Fe(II) was evident.

Strong evidence of a broad-scale 'bottom-up' fertilization effect of ash on primary production was not found locally within Reloncaví Fjord, although it is possible that the timing and peak diatom abundance of the autumn phytoplankton bloom may have shifted in response to high ash loading in the weeks following the eruption. High diatom abundances at some stations within the fjord several weeks after the eruption may have arisen from a 'top-down' effect of ash on filter feeders, although the mechanism can only be speculated herein. No clear positive

649 effect of ash deposition on chlorophyll-a was evident in the SW Atlantic, consistent with
650 expected patterns in nutrient deficiency which suggest the region to be nitrogen-limited.
651 However, in offshore waters of the SE Pacific where Fe is anticipated to limit phytoplankton
652 growth, a chlorophyll-a increase was related with maximum ash deposition and we presume
653 that this increase in chlorophyll-a was likely driven by Fe-fertilization.
654
655 **6. Data availability**
656 The complete 2015 time series from the Reloncaví Fjord mooring is available online
657 (https://figshare.com/articles/Puelo_Bouy/7754258). Source data for Figures 4-7 is included
658 in the Supplement.
659
660 **7. Acknowledgements**
661 The authors thank the Dirección de Investigación & Desarrollo UACh for its partial support
662 during this project. The data presented are part of the second chapter of the PhD Thesis of
663 MVJ at Universidad Austral de Chile. Cristian Vargas (Universidad de Concepción) is
664 thanked for making additional chlorophyll a data available, Manuel Díaz for providing Fig.
665 1 and Miriam Beck for assistance with Fe(II) flow injection analysis.
666
667 **8. Funding**
668 JLI and EA gratefully acknowledge funding from the European Commission (OCEAN-
669 CERTAIN, FP7- ENV- 2013-6.1-1; no: 603773). JLI received funding by CONICYT-
670 FONDECYT 1141065 and is partially funded by Center IDEAL (FONDAP 15150003).
671 Partial funding came from CONICYT-FONDECYT 1140385 (RT). MVJ received financial
672 support from a CONICYT Scholarship (Beca Doctorado Nacional 2015 No 21150285). IR

673 and MH received funding from the Deutsche Forschungsgemeinschaft as part of
674 Sonderforschungsbereich (SFB) 754: 'Climate-Biogeochemistry Interactions in the Tropical
675 Ocean'.
676

677 **9. Author contributions**

678 MVJ, MH, JLI and EA designed the study. MVJ, IR, MH, RT and BR conducted analytical
679 and field work. TB conducted satellite data analysis. MV, MH and TB wrote the initial
680 manuscript with all authors contributing to its revision.
681

682 **10. References**
683

684 Achterberg, E. ., Moore, C. M., Henson, S. A., Steigenberger, S., Stohl, A., Eckhardt, S.,
685 Avendano, L. C., Cassidy, M., Hembury, D., Klar, J. K., Lucas, M. I., MacEy, A. I.,
686 Marsay, C. M. and Ryan-Keogh, T. J.: Natural iron fertilization by the Eyjafjallajokull
687 volcanic eruption, Geophys. Res. Lett., 40(5), 921–926, doi:10.1002/grl.50221, 2013.
688 Ahumada, R., Rudolph, A., Gonzalez, E., Fones, G., Saldias, G. and Ahumada Rudolph, R.:
689 Dissolved trace metals in the water column of Reloncavi Fjord, Chile, Lat. Am. J. Aquat.
690 Res., 39, 567–574, doi:10.3856/vol39-issue3-fulltext-16, 2011.
691 Ayris, P. and Delmelle, P.: Volcanic and atmospheric controls on ash iron solubility: A
692 review, Phys. Chem. Earth, doi:10.1016/j.pce.2011.04.013, 2012.
693 Balseiro, E., Souza, M. S., Olabuenaga, I. S., Wolinski, L., Navarro, M. B.,
694 Laspoumaderes, C. and Modenutti, B.: Effect of the Puyehue-Cordon Caulle volcanic
695 complex eruption on crustacean zooplankton of Andean Lakes, Ecol. Austral, 2014.
696 Bonnet, S., Guieu, C., Bruyant, F., Prášil, O., Van Wambeke, F., Raimbault, P., Moutin, T.,

Grob, C., Gorbunov, M. Y., Zehr, J. P., Masquelier, S. M., Garczarek, L. and Claustre, H.: Nutrient limitation of primary productivity in the Southeast Pacific (BIOSOPE cruise), Biogeosciences, 5(1), 215–225, doi:10.5194/bg-5-215-2008, 2008.

Boyle, E. A., Edmond, J. M. and Sholkovitz, E. R.: Mechanism of iron removal in estuaries, Geochim. Cosmochim. Acta, 41(9), 1313–1324, doi:10.1016/0016-7037(77)90075-8, 1977.

Browning, T. J., Bouman, H. A., Henderson, G. M., Mather, T. A., Pyle, D. M., Schlosser, C., Woodward, E. M. S. and Moore, C. M.: Strong responses of Southern Ocean phytoplankton communities to volcanic ash, Geophys. Res. Lett., 41(8), 2851–2857, doi:10.1002/2014GL059364, 2014.

Browning, T. J., Stone, K., Bouman, H., Mather, T. A., Pyle, D. M., Moore, M. and Martinez-Vicente, V.: Volcanic ash supply to the surface ocean – remote sensing of biological responses and their wider biogeochemical significance, Front. Mar. Sci., 2, doi:10.3389/fmars.2015.00014, 2015.

Brzezinski, M. A.: The Si:C:N ratio of marine diatoms: interspecific variability and the effect of some environmental variables, J. Phycol., 21(3), 347–357, doi:10.1111/j.0022-3646.1985.00347.x, 1985.

Buck, C. S., Landing, W. M. and Resing, J.: Pacific Ocean aerosols: Deposition and solubility of iron, aluminum, and other trace elements, Mar. Chem., 157, 117–130, doi:10.1016/j.marchem.2013.09.005, 2013.

Castillo, M. I., Cifuentes, U., Pizarro, O., Djurfeldt, L. and Caceres, M.: Seasonal hydrography and surface outflow in a fjord with a deep sill: The Reloncaví fjord, Chile, Ocean Sci., 12, 533–544, doi:10.5194/os-12-533-2016, 2016.

DeGrandpre, M. D., Hammar, T. R., Smith, S. P. and Sayles, F. L.: In situ measurements of

seawater pCO2, Limnol. Oceanogr., 40(5), 969–975, doi:10.4319/lo.1995.40.5.0969, 1995.
DeGrandpre, M. D., Baehr, M. M. and Hammar, T. R.: Calibration-free optical chemical sensors, Anal. Chem., 71(6), 1152–1159, doi:10.1021/ac9805955, 1999.
Delmelle, P., Lambert, M., Dufrêne, Y., Gerin, P. and Óskarsson, N.: Gas/aerosol-ash interaction in volcanic plumes: New insights from surface analyses of fine ash particles, Earth Planet. Sci. Lett., 259, 159–170, doi:10.1016/j.epsl.2007.04.052, 2007.
Duggen, S., Croot, P., Schacht, U. and Hoffmann, L.: Subduction zone volcanic ash can fertilize the surface ocean and stimulate phytoplankton growth: Evidence from biogeochemical experiments and satellite data, Geophys. Res. Lett., doi:10.1029/2006GL027522, 2007.
Duggen, S., Olgun, N., Croot, P., Hoffmann, L., Dietze, H., Delmelle, P. and Teschner, C.: The role of airborne volcanic ash for the surface ocean biogeochemical iron-cycle: a review, Biogeosciences, 7(3), 827–844, doi:10.5194/bg-7-827-2010, 2010.
Van Eaton, A. R., Amigo, Á., Bertin, D., Mastin, L. G., Giacosa, R. E., González, J., Valderrama, O., Fontijn, K. and Behnke, S. A.: Volcanic lightning and plume behavior reveal evolving hazards during the April 2015 eruption of Calbuco volcano, Chile, Geophys. Res. Lett., 43(7), 3563–3571, doi:10.1002/2016GL068076, 2016.
Ermolin, M. S., Fedotov, P. S., Malik, N. A. and Karandashev, V. K.: Nanoparticles of volcanic ash as a carrier for toxic elements on the global scale, Chemosphere, 200, 16–22, doi:10.1016/j.chemosphere.2018.02.089, 2018.
Frogner, P., Gislason, S. R. and Oskarsson, N.: Fertilizing potential of volcanic ash in ocean surface water, Geology, 29(6), 487–490, doi:10.1130/0091-7613(2001)029<0487:fpovai>2.0.co;2, 2001.
Gledhill, M. and Buck, K. N.: The organic complexation of iron in the marine environment:

745 a review, Front. Microbiol., 3, 69, doi:10.3389/fmicb.2012.00069, 2012.
746 González, H. E., Calderón, M. J., Castro, L., Clement, A., Cuevas, L. A., Daneri, G., Iriarte,
747 J. L., Lizárraga, L., Martínez, R., Menschel, E., Silva, N., Carrasco, C., Valenzuela, C.,
748 Vargas, C. A. and Molinet, C.: Primary production and plankton dynamics in the Reloncaví
749 Fjord and the Interior Sea of Chiloé, Northern Patagonia, Chile, Mar. Ecol. Prog. Ser., 402,
750 13–30, 2010.
751 Hamme, R. C., Webley, P. W., Crawford, W. R., Whitney, F. A., Degrandpre, M. D.,
752 Emerson, S. R., Eriksen, C. C., Giesbrecht, K. E., Gower, J. F. R., Kavanaugh, M. T., Pea,
753 M. A., Sabine, C. L., Batten, S. D., Coogan, L. A., Grundle, D. S. and Lockwood, D.:
754 Volcanic ash fuels anomalous plankton bloom in subarctic northeast Pacific, Geophys. Res.
755 Lett., 37(19), L19604, doi:10.1029/2010GL044629, 2010.
756 Haraldsson, C., Anderson, L. G., Hassellöv, M., Hulth, S. and Olsson, K.: Rapid, high-
757 precision potentiometric titration of alkalinity in ocean and sediment pore waters, Deep Sea
758 Res. Part I Oceanogr. Res. Pap., 44(12), 2031–2044, doi:10.1016/S0967-0637(97)00088-5,
759 1997.
760 Hoffmann, L. J., Breitbarth, E., Ardelan, M. V., Duggen, S., Olgun, N., Hassellöv, M. and
761 Wängberg, S.-Å.: Influence of trace metal release from volcanic ash on growth of
762 Thalassiosira pseudonana and Emiliania huxleyi, Mar. Chem., 132–133, 28–33,
763 doi:10.1016/j.marchem.2012.02.003, 2012.
764 Hopwood, M. J., Santana-González, C., Gallego-Urrea, J., Sanchez, N., Achterberg, E. P.,
765 Ardelan, M. V., Gledhill, M., González-Dávila, M., Hoffmann, L., Leiknes, Ø., Magdalena
766 Santana-Casiano, J., Tsagaraki, T. M. and Turner, D.: Fe(II) stability in coastal seawater
767 during experiments in Patagonia, Svalbard, and Gran Canaria, Biogeosciences,
768 doi:10.5194/bg-17-1327-2020, 2020.

769 Horwell, C. J., Fenoglio, I., Vala Ragnarsdottir, K., Sparks, R. S. J. and Fubini, B.: Surface
770 reactivity of volcanic ash from the eruption of Soufrière Hills volcano, Montserrat, West
771 Indies with implications for health hazards, Environ. Res., 93(2), 202–215,
772 doi:10.1016/S0013-9351(03)00044-6, 2003.
773 Hoshyaripour, G. A., Hort, M. and Langmann, B.: Ash iron mobilization through
774 physicochemical processing in volcanic eruption plumes: A numerical modeling approach,
775 Atmos. Chem. Phys., 15, 9361–9379, doi:10.5194/acp-15-9361-2015, 2015.
776 Hu, C., Lee, Z. and Franz, B.: Chlorophyll aalgorithms for oligotrophic oceans: A novel
777 approach based on three-band reflectance difference, J. Geophys. Res. Ocean., 117(C1),
778 doi:10.1029/2011JC007395, 2012.
779 Iriarte, J. L., González, H. E., Liu, K. K., Rivas, C. and Valenzuela, C.: Spatial and
780 temporal variability of chlorophyll and primary productivity in surface waters of southern
781 Chile (41.5–43° S), Estuar. Coast. Shelf Sci., 74(3), 471–480,
782 doi:10.1016/j.ecss.2007.05.015, 2007.
783 Jones, M. R., Nightingale, P. D., Turner, S. M. and Liss, P. S.: Adaptation of a load-inject
784 valve for a flow injection chemiluminescence system enabling dual-reagent injection
785 enhances understanding of environmental Fenton chemistry, Anal. Chim. Acta, 796, 55–60,
786 doi:10.1016/j.aca.2013.08.003, 2013.
787 Jones, M. T. and Gislason, S. R.: Rapid releases of metal salts and nutrients following the
788 deposition of volcanic ash into aqueous environments, Geochim. Cosmochim. Acta, 72(15),
789 3661–3680, doi:10.1016/j.gca.2008.05.030, 2008.
790 Labbé-Ibáñez, P., Iriarte, J. L. and Pantoja, S.: Respuesta del microfitoplancton a la adición
791 de nitrato y ácido silícico en fiordos de la Patagonia chilena, Lat. Am. J. Aquat. Res., 43(1),
792 80–93, doi:10.3856/vol43-issue1-fulltext-8, 2015.

793 Langmann, B., Zakšek, K., Hort, M. and Duggen, S.: Volcanic ash as fertiliser for the
794 surface ocean, Atmos. Chem. Phys., 10, 3891–3899, doi:10.5194/acp-10-3891-2010, 2010.
795 León-Muñoz, J., Marcé, R. and Iriarte, J. L.: Influence of hydrological regime of an Andean
796 river on salinity, temperature and oxygen in a Patagonia fjord, Chile, New Zeal. J. Mar.
797 Freshw. Res., 47(4), 515–528, doi:10.1080/00288330.2013.802700, 2013.
798 León-Muñoz, J., Urbina, M. A., Garreaud, R. and Iriarte, J. L.: Hydroclimatic conditions
799 trigger record harmful algal bloom in western Patagonia (summer 2016), Sci. Rep., 8(1),
800 1330, doi:10.1038/s41598-018-19461-4, 2018.
801 Lin, I. I., Hu, C., Li, Y. H., Ho, T. Y., Fischer, T. P., Wong, G. T. F., Wu, J., Huang, C. W.,
802 Chu, D. A., Ko, D. S. and Chen, J. P.: Fertilization potential of volcanic dust in the low-
803 nutrient low-chlorophyll western North Pacific subtropical gyre: Satellite evidence and
804 laboratory study, Global Biogeochem. Cycles, 25, GB1006, doi:10.1029/2009GB003758,
805 2011.
806 López-Escobar, L., Parada, M. A., Hickey-Vargas, R., Frey, F. A., Kempton, P. D. and
807 Moreno, H.: Calbuco Volcano and minor eruptive centers distributed along the Liquiñe-
808 Ofqui Fault Zone, Chile (41°–42° S): contrasting origin of andesitic and basaltic magma in
809 the Southern Volcanic Zone of the Andes, Contrib. to Mineral. Petrol., 119(4), 345–361,
810 doi:10.1007/BF00286934, 1995.
811 Martin, J. H., Fitzwater, S. E. and Gordon, R. M.: Iron deficiency limits phytoplankton
812 growth in Antarctic waters, Global Biogeochem. Cycles, 4(1), 5–12, 1990.
813 Maters, E. C., Delmelle, P. and Gunnlaugsson, H. P.: Controls on iron mobilisation from
814 volcanic ash at low pH: Insights from dissolution experiments and Mössbauer
815 spectroscopy, Chem. Geol., 449, 73–81, doi:10.1016/j.chemgeo.2016.11.036, 2017.
816 Mélançon, J., Levasseur, M., Lizotte, M., Delmelle, P., Cullen, J., Hamme, R. C., Peña, A.,

817 Simpson, K. G., Scarratt, M., Tremblay, J. É., Zhou, J., Johnson, K., Sutherland, N.,
818 Arychuk, M., Nemcek, N. and Robert, M.: Early response of the northeast subarctic Pacific
819 plankton assemblage to volcanic ash fertilization, Limnol. Oceanogr., 59,
820 doi:10.4319/lo.2014.59.1.0055, 2014.
821 Millero, F. J., Sotolongo, S. and Izaguirre, M.: The oxidation kinetics of Fe(II) in seawater,
822 Geochim. Cosmochim. Acta, 51(4), 793–801, doi:10.1016/0016-7037(87)90093-7, 1987.
823 Molinet, C., Díaz, M., Marín, S. L., Astorga, M. P., Ojeda, M., Cares, L. and Asencio, E.:
824 Relation of mussel spatfall on natural and artificial substrates: Analysis of ecological
825 implications ensuring long-term success and sustainability for mussel farming,
826 Aquaculture, 467, 211–218, doi:10.1016/j.aquaculture.2016.09.019, 2017.
827 Moore, C. M., Mills, M. M., Arrigo, K. R., Berman-Frank, I., Bopp, L., Boyd, P. W.,
828 Galbraith, E. D., Geider, R. J., Guieu, C., Jaccard, S. L., Jickells, T. D., La Roche, J.,
829 Lenton, T. M., Mahowald, N. M., Maranon, E., Marinov, I., Moore, J. K., Nakatsuka, T.,
830 Oschlies, A., Saito, M. A., Thingstad, T. F., Tsuda, A. and Ulloa, O.: Processes and
831 patterns of oceanic nutrient limitation, Nat. Geosci, 6(9), 701–710, doi:10.1038/ngeo1765,
832 2013.
833 Morton, P. L., Landing, W. M., Hsu, S. C., Milne, A., Aguilar-Islas, A. M., Baker, A. R.,
834 Bowie, A. R., Buck, C. S., Gao, Y., Gichuki, S., Hastings, M. G., Hatta, M., Johansen, A.
835 M., Losno, R., Mead, C., Patey, M. D., Swarr, G., Vandermark, A. and Zamora, L. M.:
836 Methods for the sampling and analysis of marine aerosols: Results from the 2008
837 GEOTRACES aerosol intercalibration experiment, Limnol. Oceanogr. Methods, 11,
838 doi:10.4319/lom.2013.11.62, 2013.
839 Mosley, L. M., Husheer, S. L. G. and Hunter, K. A.: Spectrophotometric pH measurement
840 in estuaries using thymol blue and m-cresol purple, Mar. Chem., 91, 175–186,

841 doi:10.1016/j.marchem.2004.06.008, 2004.
842 Newcomb, T. W. and Flagg, T. A.: Some effects of Mt. St. Helens volcanic ash on juvenile
843 salmon smolts., Mar. Fish. Rev., 45(2), 8–12, 1983.
844 Olsson, J., Stipp, S. L. S., Dalby, K. N. and Gislason, S. R.: Rapid release of metal salts and
845 nutrients from the 2011 Grímsvötn, Iceland volcanic ash, Geochim. Cosmochim. Acta,
846 doi:10.1016/j.gca.2013.09.009, 2013.
847 Rapp, I., Schlosser, C., Rusiecka, D., Gledhill, M. and Achterberg, E. P.: Automated
848 preconcentration of Fe, Zn, Cu, Ni, Cd, Pb, Co, and Mn in seawater with analysis using
849 high-resolution sector field inductively-coupled plasma mass spectrometry, Anal. Chim.
850 Acta, 976, 1–13, doi:10.1016/j.aca.2017.05.008, 2017.
851 Rogan, N., Achterberg, E. P., Le Moigne, F. A. C., Marsay, C. M., Tagliabue, A. and
852 Williams, R. G.: Volcanic ash as an oceanic iron source and sink, Geophys. Res. Lett.,
853 43(6), 2732–2740, doi:10.1002/2016GL067905, 2016.
854 Romero, J. E., Morgavi, D., Arzilli, F., Daga, R., Caselli, A., Reckziegel, F., Viramonte, J.,
855 Díaz-Alvarado, J., Polacci, M., Burton, M. and Perugini, D.: Eruption dynamics of the 22–
856 23 April 2015 Calbuco Volcano (Southern Chile): Analyses of tephra fall deposits, J.
857 Volcanol. Geotherm. Res., 317, 15–29, doi:10.1016/j.jvolgeores.2016.02.027, 2016.
858 Sanchez, N., Bizsel, N., Iriarte, J. L., Olsen, L. M. and Ardelan, M. V.: Iron cycling in a
859 mesocosm experiment in a north Patagonian fjord: Potential effect of ammonium addition
860 by salmon aquaculture, Estuar. Coast. Shelf Sci., 220, 209–219,
861 doi:10.1016/j.ecss.2019.02.044, 2019.
862 Santana-Casiano, J. M., Gonzaalez-Davila, M. and Millero, F. J.: Oxidation of nanomolar
863 levels of Fe(II) with oxygen in natural waters, Environ. Sci. Technol., 39(7), 2073–2079,
864 doi:10.1021/es049748y, 2005.

865 Sarmiento, J. L.: Atmospheric CO2 stalled, Nature, doi:10.1038/365697a0, 1993.
866 Sarthou, G., Bucciarelli, E., Chever, F., Hansard, S. P., Gonzalez-Davila, M., Santana-
867 Casiano, J. M., Planchon, F. and Speich, S.: Labile Fe(II) concentrations in the Atlantic
868 sector of the Southern Ocean along a transect from the subtropical domain to the Weddell
869 Sea Gyre, Biogeosciences, 8(9), 2461–2479, doi:10.5194/bg-8-2461-2011, 2011.
870 Seidel, M. P., DeGrandpre, M. D. and Dickson, A. G.: A sensor for in situ indicator-based
871 measurements of seawater pH, Mar. Chem., 109(1), 18–28,
872 doi:10.1016/j.marchem.2007.11.013, 2008.
873 Siringan, F. P., Racasa, E. D. R., David, C. P. C. and Saban, R. C.: Increase in Dissolved
874 Silica of Rivers Due to a Volcanic Eruption in an Estuarine Bay (Sorsogon Bay,
875 Philippines), Estuaries and Coasts, 41, 2277–2288, doi:10.1007/s12237-018-0428-1, 2018.
876 Stewart, C., Johnston, D. M., Leonard, G. S., Horwell, C. J., Thordarson, T. and Cronin, S.
877 J.: Contamination of water supplies by volcanic ashfall: A literature review and simple
878 impact modelling, J. Volcanol. Geotherm. Res., 158(3), 296–306,
879 doi:10.1016/j.jvolgeores.2006.07.002, 2006.
880 Sunda, W. G., Buffle, J. and Van Leeuwen, H. P.: Bioavailability and Bioaccumulation of
881 Iron in the Sea, in The Biogeochemistry of Iron in Seawater, vol. 7, edited by D. R. Turner
882 and K. A. Hunter, pp. 41–84, John Wiley & Sons, Ltd, Chichester., 2001.
883 Torres, R. and Ampuero, P.: Strong CO2 outgassing from high nutrient low chlorophyll
884 coastal waters off central Chile (30°S): The role of dissolved iron, Estuar. Coast. Shelf Sci.,
885 83(2), 126–132, doi:10.1016/j.ecss.2009.02.030, 2009.
886 Torres, R., Silva, N., Reid, B. and Frangopulos, M.: Silicic acid enrichment of subantarctic
887 surface water from continental inputs along the Patagonian archipelago interior sea (41-
888 56°S), Prog. Oceanogr., 129, 50–61, doi:10.1016/j.pocean.2014.09.008, 2014.

889 Utermöhl, H.: Zur Vervollkommnung der quantitativen Phytoplankton-Methodik, SIL
890 Commun. 1953-1996, doi:10.1080/05384680.1958.11904091, 1958.
891 Vergara-Jara, M. J., DeGrandpre, M. D., Torres, R., Beatty, C. M., Cuevas, L. A., Alarcón,
892 E. and Iriarte, J. L.: Seasonal Changes in Carbonate Saturation State and Air-Sea CO2
893 Fluxes During an Annual Cycle in a Stratified-Temperate Fjord (Reloncaví Fjord, Chilean
894 Patagonia), J. Geophys. Res. Biogeosciences, 124(9), 2851–2865,
895 doi:10.1029/2019JG005028, 2019.
896 Watson, A. J.: Volcanic iron, CO2, ocean productivity and climate, Nature,
897 doi:10.1038/385587b0, 1997.
898 Weinbauer, M. G., Guinot, B., Migon, C., Malfatti, F. and Mari, X.: Skyfall - neglected
899 roles of volcano ash and black carbon rich aerosols for microbial plankton in the ocean, J.
900 Plankton Res., 39(2), 187–198, doi:10.1093/plankt/fbw100, 2017.
901 Welschmeyer, N. A.: Fluorometric analysis of chlorophyll a in the presence of chlorophyll
902 b and pheopigments, Limnol. Oceanogr., 39(8), 1985–1992,
903 doi:10.4319/lo.1994.39.8.1985, 1994.
904 Witham, C. S., Oppenheimer, C. and Horwell, C. J.: Volcanic ash-leachates: a review and
905 recommendations for sampling methods, J. Volcanol. Geotherm. Res., 141(3), 299–326,
906 doi:10.1016/j.jvolgeores.2004.11.010, 2005.
907 Wolinski, L., Laspoumaderes, C., Bastidas Navarro, M., Modenutti, B. and Balseiro, E.:
908 The susceptibility of cladocerans in North Andean Patagonian lakes to volcanic ashes,
909 Freshw. Biol., 58, 1878–1888, doi:10.1111/fwb.12176, 2013.
910 Yevenes, M. A., Lagos, N. A., Farías, L. and Vargas, C. A.: Greenhouse gases, nutrients
911 and the carbonate system in the Reloncaví Fjord (Northern Chilean Patagonia):
912 Implications on aquaculture of the mussel, Mytilus chilensis, during an episodic volcanic

913 eruption, Sci. Total Environ., doi:10.1016/j.scitotenv.2019.03.037, 2019.

914